New investigation of low-lying states in ^{12}Be via a ^{2}H(^{13}B, ^{3}He) reaction

W. Liu,[1] J. L. Lou,[1,*] Y. L. Ye,[1] S. M. Wang,[2,3] Z. W. Tan,[1] Z. H. Li,[1] Q. T. Li,[1] H. Hua,[1] X. F. Yang,[1] J. Y. Xu,[1] H. J. Ong,[4,5,6,7] D. T. Tran,[4,8] N. Aoi,[4] E. Ideguchi,[4] D. Y. Pang,[9] C. X. Yuan,[10] Y. Jiang,[1] B. Yang,[1] Y. Liu,[1] J. G. Li,[1] Z. Q. Chen,[1] J. X. Han,[1] S. W. Bai,[1] G. Li,[1] K. Ma,[1] H. Y. Zhu,[1] and B. L. Xia[1]

[1]*School of Physics and State Key Laboratory of Nuclear Physics and Technology, Peking University, Beijing 100871, China*
[2]*Key Laboratory of Nuclear Physics and Ion-beam Application (MOE), Institute of Modern Physics, Fudan University, Shanghai 200433, China*
[3]*Shanghai Research Center for Theoretical Nuclear Physics, NSFC and Fudan University, Shanghai 200438, China*
[4]*Research Centre for Nuclear Physics, Osaka University, Ibaraki, Osaka 567-0047, Japan*
[5]*Institute of Modern Physics, Chinese Academy of Sciences, Lanzhou 730000, China*
[6]*Joint Department for Nuclear Physics, Lanzhou University and Institute of Modern Physics, Chinese Academy of Sciences, Lanzhou 730000, China*
[7]*School of Nuclear Science and Technology, University of Chinese Academy of Sciences, Beijing 100049, China*
[8]*Institute of Physics, Vietnam Academy of Science and Technology, Hanoi 10000, Vietnam*
[9]*School of Physics, Beijing Key Laboratory of Advanced Nuclear Materials and Physics, Beihang University, Beijing 100191, China*
[10]*Sino-French Institute of Nuclear Engineering and Technology, Sun Yat-Sen University, Zhuhai 519082, China*

(Received 14 December 2021; revised 23 February 2022; accepted 7 March 2022; published 21 March 2022)

We investigate the low-lying positive-parity states in ^{12}Be, which are populated by the ^{2}H(^{13}B, ^{3}He) reaction via $l = 1$ proton transfer for the first time using a radioactive beam ^{13}B at 23 MeV/nucleon. Spectroscopic factors and excitation energies of these states are in reasonable agreement with the shell model predictions. Besides two bound states, we observe a resonant state at $E_x = 4.8 \pm 0.1$ MeV with an intrinsic width of 0.42 ± 0.28 MeV, which predominately decays via one neutron to the bound states in ^{11}Be. It most likely corresponds to the $E_n = 1.24$ MeV state observed in the previous one-proton removal reaction. The spin-parity of 2^+ is tentatively assigned to this resonance according to the analysis of its angular distributions as well as the theoretical calculations, including shell model and Gamow coupled-channel approach.

DOI: 10.1103/PhysRevC.105.034613

I. INTRODUCTION

With the development of accelerator and nuclear detection technologies, more and more unstable nuclei far from the β-stability line were produced. For unstable nuclei, especially those in the light-mass region, the rearrangement of some orbitals often appears, leading to the reduction or disappearance of $N = 8$ [1] shell gaps, as well as the appearance of new magic numbers at $N = 16$ [2], 32 [3], 34 [4], and so on. One of the most famous examples is the one-neutron ($1n$) halo nucleus ^{11}Be. The spin parities of its ground state (g.s.) and the first excited states are $1/2^+$ and $1/2^-$, respectively, indicating the intrusion of s orbital and the breakdown of the magic number at $N = 8$ [5–9].

^{12}Be, with one more neutron than ^{11}Be, was also intensively investigated by a variety of experiments, such as the ^{10}Be(t, p) reaction [10], the inelastic scattering of ^{12}Be [11], the ^{2}H(^{11}Be, p) reaction [12–16], the charge-exchange reaction [17], and the $1n$ [18,19] or one-proton ($1p$) [20] removal reactions and so on. The spin parities of the four bound states at excitation energies of $E_x = 0$, 2.11, 2.25, and 2.71 MeV have been firmly assigned to be 0^+_1, 2^+_1, 0^+_2, and 1^-_1, respectively. However, the experimental information of the unbound states in ^{12}Be is very scarce. Until now, only one near-threshold state at $E_x = 3.21$ MeV and two states at $E_x =$ 4.58 and 5.71 MeV were observed from the measurements of $1n$, two-neutrons ($2n$), and multiple-nucleons transfer reactions [10,16,21,22]. Their spin parities were only tentatively assigned to be 0^-, 3^-, and 4^+, respectively [16,23,24]. The energy level scheme of ^{12}Be is summarized in Fig. 1.

Another resonant state of ^{12}Be, decaying via $1n$ with an energy of $E_n = 1.24 \pm 0.021$ MeV and a width of 634 ± 60 keV, was observed from the $1p$ removal reaction of ^{13}B [20]. However, the excitation energy and spin parity of this resonant state was not finally determined. As shown in Fig. 1(c), it would be 4.412 or 4.732 MeV when it decays to the g.s. or to the first excited state of ^{11}Be. The corresponding spin parity would be most likely 2^- or 2^+ [20]. Recently, a resonance with an excitation energy of $E_x = 4.44 \pm 0.15$ MeV and a width of $0 \approx 0.43$ MeV was observed in the ^{2}H(^{11}Be, p) reaction [16]. The distorted wave Born approximation (DWBA) analysis suggested that this state was composed of a ^{11}Be core in its g.s. and a neutron with the transfer angular momentum $l = 1$. Its parity should be negative, and it might correspond to the $E_n = 1.24$ MeV state [20]. However, based on shell model calculations, Fortune pointed out that the $E_n = 1.24$ MeV

*jllou@pku.edu.cn

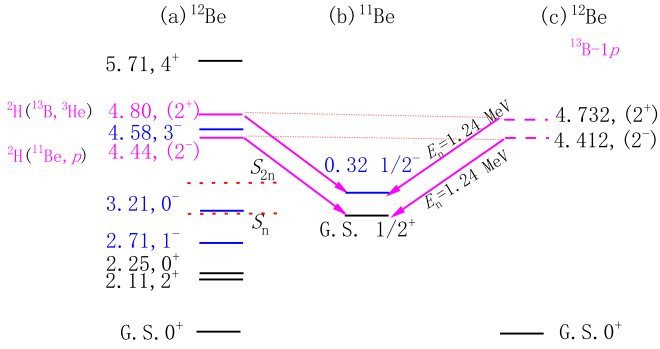

FIG. 1. Energy level scheme of (a) ^{12}Be, (b) ^{11}Be, and (c) the possible decay path of the $E_n = 1.24$ MeV state in ^{12}Be, which was observed from the $1p$ removal reaction [20]. The excitation energy of the $E_n = 1.24$ MeV state was not determined. See text for the details.

state is unlikely to be a negative-parity state because the spectroscopic factor (SF) of an s-shell proton removed from ^{13}B is very small (SF ≈ 0.01) [24–26]. Even if the core excitation components in both nuclei of ^{13}B and ^{12}Be were taken into consideration, only the first (two/three) 0^+ and 2^+ states can be populated by the $1p$ removal or transfer reactions [27]. At the same time, Fortune encouraged a new investigation of the ^{2}H(^{13}B, ^{3}He) reaction [27]. However, the calculated SFs [27] are very different from the results anticipated by Macchiavelli *et al.* with the rotational model [28] (see below). The uncertain spin-parity assignment of this resonance, ambiguous decay path, and different theoretical predictions stimulate a new investigation of the ^{2}H(^{13}B, ^{3}He) reaction.

In this paper, we report on the results of a new (d, ^{3}He) experiment performed with a radioactive beam of ^{13}B at 23 MeV/nucleon in inverse kinematics. The experimental setup is described in Sec. II. The experimental results of the ^{13}B $+d$ elastic scattering and the ^{2}H(^{13}B, ^{3}He) reaction are shown in Sec. III, followed by the corresponding theoretical calculations in Sec. IV. A brief summary is given in the last section.

II. EXPERIMENTAL SETUP

The experiment was carried out at the EN-course beam line at Research Center for Nuclear Physics (RCNP), Osaka University [29,30]. A secondary beam at 23 MeV/nucleon with a purity of 98 % and an intensity of $\approx 2.0 \times 10^4$ particles per second was produced from a 60-MeV/nucleon ^{18}O primary beam impinging on a 3.8-mm-thick ^{9}Be target, and purified by the electromagnetic separator after punching through a 3.07-mm-thick aluminium degrader. The energy spread of the secondary beam was $\Delta E/E \leqslant 1.5\%$.

Figure 2 shows the experimental setup. Two plastic scintillation detectors, F2 PL and F3 PL, which provide both the time-of-flight (TOF) and the energy losses (ΔE) of the fragments, were used to discriminate the secondary beam. The incident angles and hit positions on the targets of the ^{13}B beam were determined by two position-sensitive parallel plate avalanche chambers (PPACs) with resolutions less than 0.3° and 1.5 mm. The PPACs were installed upstream of a $(CD_2)_n$ target with a thickness of 3.98 mg/cm^2, which was rotated

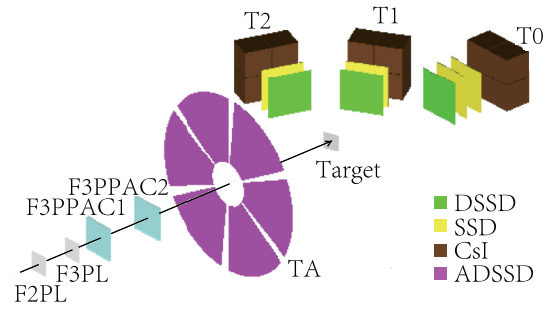

FIG. 2. Schematic view of the experimental setup.

20° relative to the beam direction to reduce the energy losses in the target of the charged particles emitting to T2 and T1 (see Fig. 2). The experimental results with a $(CH_2)_n$ target in the same experiment have been published in Ref. [31].

As plotted in Fig. 2, four sets of charged particle telescopes named T0, T1, T2, and TA were installed in a large scattering chamber to detect the projectilelike particles around the beam direction, the targetlike charged particles, the deuterons elastically scattered from ^{13}B, and the protons from the ^{2}H(^{13}B, p) ^{14}B reaction, respectively. T0, T1, and T2 were all composed of a double-sided silicon strip (DSSD) detector, one or two large surface silicon detectors (SSD), and a layer of 4-cm-thick CsI(Tl) crystals read out by photodiodes. Both DSSD (32 × 32 strips) and SSD had an active area of 64 × 64 mm^2 . T0 centered at around the beam direction, was made up of a 1000-μm-thick DSSD, two 1500-μm-thick SSDs, and a layer of CsI(Tl) detectors. T1 and T2 consisting of the same compositions, namely a 60-μm-thick DSSD, a 1500-μm-thick SSD and an array of CsI(Tl) crystals, were installed at around 31° and 70° with respect to the beam line. The distances between the center of target and the first layer of T0, T1, and T2 were 200, 150, and 150 mm, respectively. The angular and energy resolutions of T1 and T2 were 0.9° (FWHM) and less than 1% for α particles at 5.486 MeV, respectively. TA, a set of the annular double-sided silicon strip detector (ADSSD) composed of six sectors, was not involved in this paper. Please see more details about TA in Refs. [14,15].

III. EXPERIMENTAL RESULTS

A. Elastic scattering

The experiment was performed in inverse kinematics, and different reaction channels were discriminated by the coincidence detection of boron or beryllium isotopes in T0 and light particles in other telescopes. As shown in Fig. 3, protons and deuterons detected in the telescope T2 are clearly identified by the standard ΔE-E method. The inset of Fig. 3 presents the particle identification (PID) spectrum detected in T0 after gated on the recoil deuterons detected in T2. Although ^{13}B is predominant, a small amount of ^{12}B and a few ^{11}B events are also seen.

Figure 4 displays the bidimensional kinematic spectrum of the recoil deuterons in coincidence with the boron isotopes. The kinematic loci (red solid curve) well reproduce the elastic

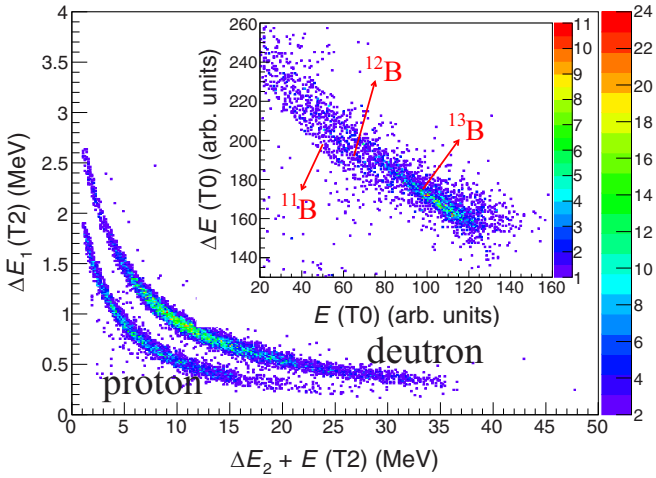

FIG. 3. Deuterons elastically scattered from ^{13}B in the particle identification (PID) spectrum measured by T2. The inset shows the PID spectrum measured by T0, where the boron isotopes are shown in coincidence with deuterons.

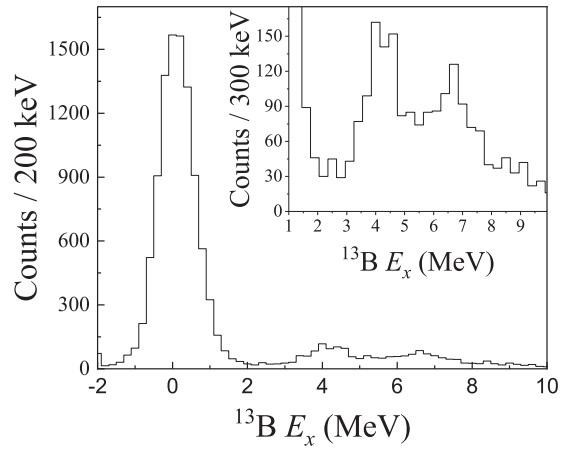

FIG. 5. Excitation energy spectrum of ^{13}B reconstructed from energies and angles of the scattered deuterons measured by T2. The inset shows more details of the energy spectrum for inelastic scattering.

scattering data of ^{13}B $+d$. Several low-lying states are observed from the inelastic scattering of ^{13}B $+d$. The excitation energy spectrum deduced from the energies and angles of the recoil deuterons detected in T2 is given in Fig. 5. The elastic scattering peak centered at around 0 MeV is evidently discriminated from other low-lying excited states.

The elastic scattering differential cross sections, as a ratio to the Rutherford cross sections, are plotted in Fig. 6. The count of the outgoing deuterons for each data point, which corresponds to an angular range of 1.5 ° (2.0 ° at small angles) in the laboratory frame, was obtained by fitting the excitation energy spectrum shown in Fig. 5. The integrated resolution of 990 keV (FWHM) is in good agreement with the simulated result using GEANT4 package [32], which considers the energy spread of the secondary beam (1.5%), the energy losses of outgoing deuterons and ^{13}B in the target, as well as the energy and angular resolutions of real experimental setup. For each data point, the width of the Gaussian peak fixed at zero was determined by the GEANT4 simulation. Only the amplitude of Gaussian function was left as a free parameter for each peak during the fitting procedure. The error bars are purely statistical. The systematic error is less than 8%, considering the uncertainties in the geometrical efficiency determination (5%), the thickness of the target (2%), and the cuts on the PID spectrum (5%) shown in Fig. 3.

The $(CD_2)_n$ target is made from deuterated polyethylene, which is usually contaminated by the hydrogen components. Following the procedure described in Refs. [33,34], the

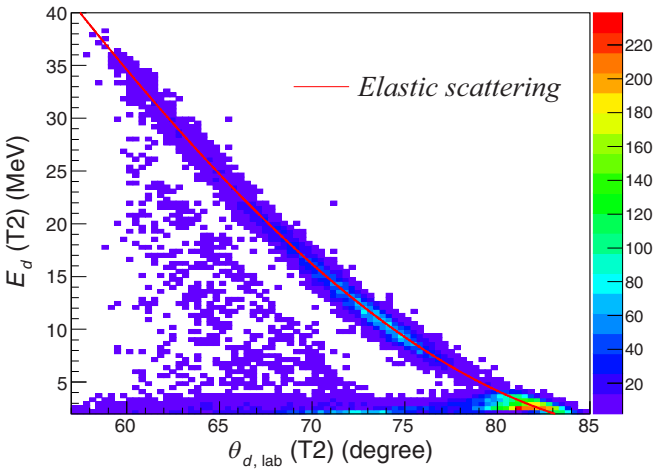

FIG. 4. Bidimensional plot of energy vs angle in the laboratory frame for the recoil deuterons in coincidence with the boron isotopes at forward angles. The kinematic loci for the elastic scattering of ^{13}B $+d$ are shown as the red solid curve.

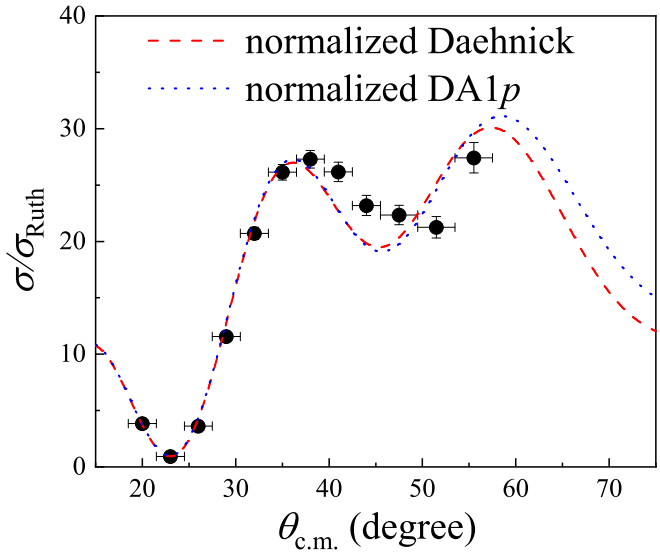

FIG. 6. Elastic scattering differential cross sections, relative to the Rutherford cross sections. Two sets of global optical potentials were employed for the theoretical calculations. See text for more details.

TABLE I. Parameters of the optical model potentials for the elastic scattering and ^{2}H(^{13}B, ^{3}He)^{12}Be reaction calculations.

Channel	V_V (MeV)	r_V (fm)	a_V (fm)	W_V (MeV)	r_W (fm)	a_W (fm)	W_S (MeV · fm)	r_{W_S} (fm)	a_{W_S} (fm)	$V_{s.o.}$ (fm)	$r_{s.o.}$ (fm)	$a_{s.o.}$ (fm)	r_C (fm)	χ^2/n
^{13}B + d (Daehnick)	76.766	1.170	0.788	2.741	1.325	0.655	11.467	1.325	0.655	2.994	1.070	0.660	1.300	5.08
^{13}B + d (DA1p)	83.287	1.063	0.776	10.898	1.785	0.744	0.011	1.785	0.744	0.000	–	–	1.300	7.09
^{12}Be + ^{3}He	114.214	1.090	0.815	3.316	1.256	0.840	23.052	1.256	0.840	0.000	–	–	1.300	

percentage of contaminated hydrogen component was determined to be $11.5 \pm 0.3\%$. The error 0.3% was deduced from the statistics of the numbers of the scattered light particle and the incoming beam particles.

In the framework of optical model, two sets of global optical potentials (OPs), Daehnick [35] and DA1p [36], were applied to describe the elastic scattering data of ^{13}B + d using the code FRESCO [37]. To better describe the experimental data, the best depths of the real (V_V) and the imaginary part ($W_V + W_S$) were searched with the χ^2 minimization method. The geometric parameters r and a were not varied and were those of the global OPs. Both OPs can well reproduce the current data, as shown in Fig. 6. The best optical potential parameters and the corresponding χ^2/n values are listed in Table I.

B. ^{2}H(^{13}B, ^{3}He)^{12}Be transfer reaction

The analysis of differential cross sections of the ^{2}H(^{13}B, ^{3}He) reaction is based on the coincidence of ^{3}He measured in T1 and beryllium isotopes detected in T0. The 1n (2n) separation threshold of ^{12}Be is $S_n = 3.1707$ ($S_{2n} = 3.672$) MeV. For the states with excitation energies above theses thresholds, which are populated by the ^{2}H(^{13}B, ^{3}He) reaction would emit 1n or 2n, and ^{11}Be or ^{10}Be would be detected in the telescope T0. Figure 7 exhibits the beryllium isotopes detected by T0, with a gate of ^{3}He measured in T1. ^{10}Be, ^{11}Be, and ^{12}Be are evidently observed. The helium isotopes detected in T1 are shown in the inset of Fig. 7.

Figure 8 illustrates the energies vs angles for ^{3}He measured by T1 in coincidence with the beryllium isotopes emitting to T0. The energy losses of ^{3}He in the target were corrected in Fig. 8, assuming a reaction point at the middle of the target. The excitation energy spectrum of ^{12}Be, as shown in Fig. 9, was reconstructed from the energy and angle of ^{3}He with a gate of the beryllium isotopes. Three peaks are observed in the region of $E_x < 7$ MeV. The first peak is around zero, corresponding to the g.s. of ^{12}Be. The second peak at around $E_x = 2.2$ MeV should be a mixture of the 0_2^+ (2.251 MeV) and 2_1^+ (2.109 MeV) excited states. As stated above, the 2.71-MeV state with a spin-parity of 1^- is ruled out from the second peak because the negative-parity states are unlikely to be populated in the proton-removal or the proton-transfer reaction [26]. For the third peak, the excitation energy at around $E_x = 4.8$ MeV is above both 1n and 2n separation thresholds of ^{12}Be. Most events of this peak were observed from the coincidence of ^{3}He and ^{11}Be rather than ^{10}Be, demonstrating it predominantly decays to the bound states of ^{11}Be, referred to as the g.s. or the first excited state at $E_x = 320$ keV. The relative branching ratio of the 1n and 2n decay channels was determined to be $84 \pm 14\%$ by calculating the ratio of the ^{3}He counts in coincidence with ^{11}Be and ^{10}Be ions. Note that the yield of

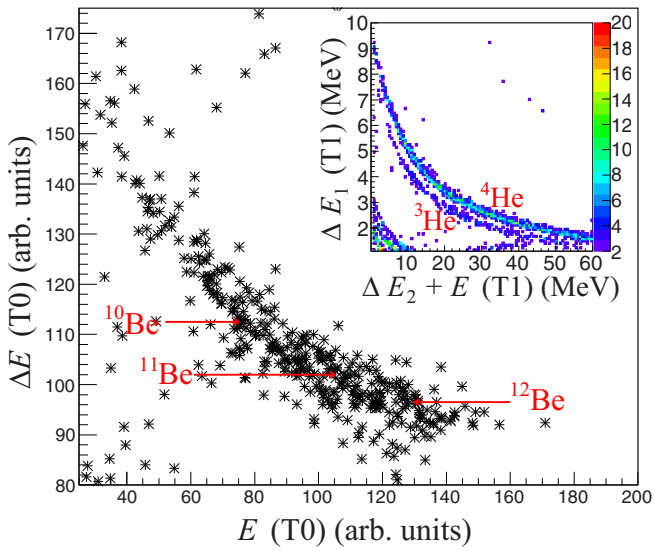

FIG. 7. PID spectrum of the beryllium isotopes detected by T0 in coincidence with the light charged particles measured in T1. The inset shows the measured helium isotopes by T1.

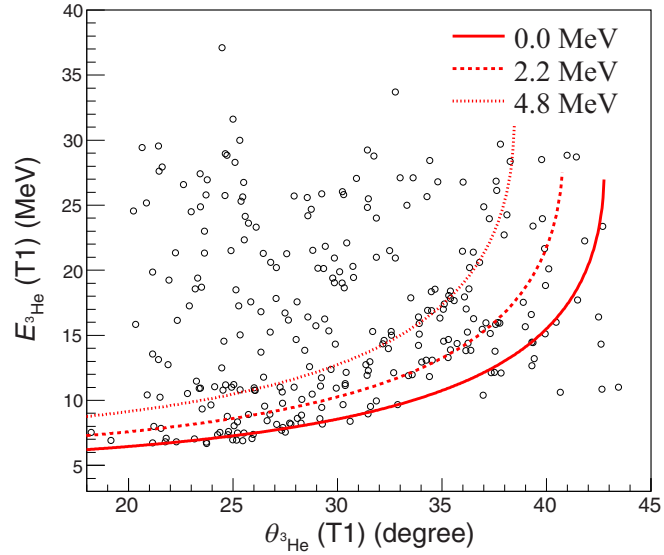

FIG. 8. In coincidence with the beryllium isotopes, the energies of ^{3}He as a function of angles in the laboratory frame. The red lines illustrate the calculated kinematics of the ^{2}H(^{13}B, ^{3}He)^{12}Be transfer reaction to the states of interest in ^{12}Be.

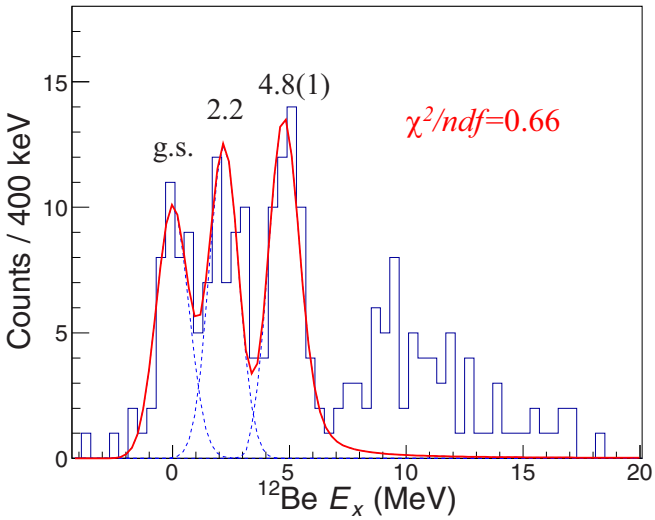

FIG. 9. Excitation energy spectrum of ^{12}Be reconstructed from the energies and angles of ^{3}He at 24-44°. The blue dashed curves show the fitted peaks for each state, and the red solid curve shows the sum of blue dashed curves. The number of degrees of freedom (ndf) corresponds to the number of data points used in the fit minus the number of free parameters.

^{10}Be includes possible contributions from directly populated the resonances in ^{11}Be that subsequently decay to ^{10}Be via emitting $1n$. The decaying path predominated by $1n$ is similar to the $E_n = 1.24$ MeV state [20].

As displayed in Fig. 9, the spectrum was fitted with three peaks in the region of $E_x < 7$ MeV. In this experiment, both the energy and the time information of each detector were recorded. Time cut was used when we analyzed the excitation energy spectrum from the coincidence events to reduce the random coincidence events. The background contributions from reactions with carbon in the physical target of $(CD_2)_n$ were verified to be negligible via the analysis of run files using the carbon and empty targets. Thus, no background was included in the fitting functions.

The Gaussian and Breit-Wigner functions [16,38] were convoluted with the response function of the whole detection system to fit the bound and unbound states in ^{12}Be, respectively. The response function of the present detection system was simulated using GEANT4 package, taking into consideration the energy spread of secondary beam (1.5%), the energy losses of ^{3}He in the target, the detection threshold and dead areas of various detectors, the energy (including the noise of detection system and the statistical fluctuation for different deposited energy, which is characterized by Fano factor), and angular resolution (0.9°) of the real experimental setup. An integrated energy resolution of 0.69–0.57 MeV (FWHM) was obtained for the states in the excitation energy range of $E_x =$ 0.0-6.0 MeV. For the two bound states, only the amplitudes were left as free parameters while the peak positions were fixed at 0 and 2.2 MeV and their widths were deduced from the response function.

For the resonance, the Breit-Wigner function $F(E_r)$ with an energy-dependent width $\Gamma(E_r)$ is defined as [16,38]:

$$F(E_r) = \frac{\Gamma(E_r)}{(E_x - E_0)^2 + \Gamma^2(E_r)/4}, \quad (1)$$

where E_r is the relative energy of the decay particles, E_0 and E_x are the centroid energy and the excitation energy of the resonant peak, respectively. Note that the resonant state predominantly decays by $1n$ to the first excited state in ^{11}Be rather than $2n$ to ^{10}Be. The relationship between E_r and E_x is $E_x = E_r + S_n + 0.32$, where $S_n = 3.1707$ MeV is the $1n$ separation energy of ^{12}Be and 0.32 MeV is the excitation energy of the first excited state in ^{11}Be. The energy-dependent width is defined as $\Gamma(E_r) \equiv g\sqrt{E_r}$, where g is a free parameter during the fitting procedure. Based on the χ^2 minimization method, the centroid and the intrinsic width of this resonant state are fitted to be 4.8 ± 0.1 MeV and 0.42 ± 0.28 MeV, respectively.

To obtain the differential cross sections, the excitation energy spectra were fitted every five degrees in the laboratory frame. Differential cross sections for these three peaks are shown in Fig. 10. The error bars are purely statistical. The systematic error is less than 10 %, taking into consideration the uncertainties in the geometrical efficiency determination (5%), the thickness of the target (2%), and the cuts of ^{3}He (5%) and the boron isotopes (5%) on the PID spectra shown in Fig. 7.

The DWBA calculations with different transferred orbital angular momentum, namely $l = 1$ and $l = 0$, were performed with the codes FRESCO [37] and TWOFNR [39] using the finite-range transfer interactions. Normalized Daehnick potential parameters deduced from the elastic scattering differential cross sections were adopted for the entrance channel, considering the relatively smaller χ^2/n value comparing with the normalized DA1p potential. Systematic OP parameters of GDP08 [40], which was developed by Pang *et al.* for the $A = 3$ projectiles, were used for the exit channel. All the optical potential parameters are listed in Table I. The depths of binding potentials were adjusted to reproduce the $1p$ binding energy of ^{13}B. The other parameters were set to default values, such as $r = 1.25$ fm, $a = 0.65$ fm. Comparing the experimental differential cross sections to the DWBA calculations, the experimental SFs were determined and summarized in Table II. The uncertainties for the SFs correspond to a 68% confidence level with $\chi^2_{\min} + 1$. As listed in Table II, the difference between the SFs extracted from the results of FRESCO (SF_{FRESCO}) and TWOFNR (SF_{TWOFNR}) is less than 15%. Note that the calculated differential cross sections in Fig. 10 have been averaged over an angular range corresponding to the angular acceptance for each data point and been multiplied by the corresponding experimental SFs.

For the bound excited states as displayed in Figs. 10(a) and 10(b), the DWBA calculations with the $l = 1$ proton transfer well describe the experimental angular distributions. As an example, in Fig. 10(c), the DWBA calculation with the transferred proton angular momentum $l = 0$ is illustrated as the black dotted curve. The $l = 0$ curve could not give a good reproduction of the angular distributions, and thus produces a very large χ^2 value ($\chi^2 = 17.70$). The $l = 1$ curves are

TABLE II. Excitation energies and SFs for the low-lying states in ^{12}Be. The experimental SFs are extracted from the present ^{2}H(^{13}B, ^{3}He) reaction and the corresponding uncertainties are from the fit to the differential cross sections for each state based on the χ^2 minimization method. Comparing with the experimental results, the shell model calculation results with the latest YSOX interaction [41], as well as the results obtained by Fortune [27] and Macchiavelli *et al.* [28] are also given. The excitation energies and the intrinsic width of low-lying states in ^{12}Be predicted by the GCC approach [42] are comparably listed.

	Expt.			YSOX [41]		Fortune [27]		Macchiavelli *et al.* [28]		GCC [42]	
J^π	E_x (MeV)	SF_{TWOFNR}	SF_{FRESCO}	E_x (MeV)	SF	E_x (MeV)	SF[a]	E_x (MeV)	SF	E_x (MeV)	Γ (MeV)
0_1^+	0.000	0.49(8)	0.43(7)	0.000	0.28	0.0	0.60	0.0	0.50	0.000	
2_1^+	2.109	0.60(11)	0.62(11)	2.446	0.28	2.11	0.36	2.11	0.50	2.33	
0_2^+	2.251			2.779	0.17	2.25	0.10	2.25	0.00	2.54	
2_2^+	4.8(1)[b]	1.49(20)	1.45(19)	5.078	1.74	≈5	1.46			4.80	0.091
0_3^+				5.565	0.01	4.8	small			4.84[c]	0.513
2^-			5.152 [16]	<0.01	5.120 [24]	≈ 0.01 [26]			4.515	0.814	

[a]The values were calculated from SF = SF_{1p} × SF/SF_{1p}, where SF/SF_{1p} was given in Table 1 of Ref. [27], and SF_{1p} was 0.7 and 2.5 for the 0^+ and 2^+ state, respectively [27].
[b]The spin parity of this resonance is tentatively assigned in this work.
[c]The excitation energy and intrinsic width of 0_4^+, while they are 3.57 and 0.046 MeV of 0_3^+.

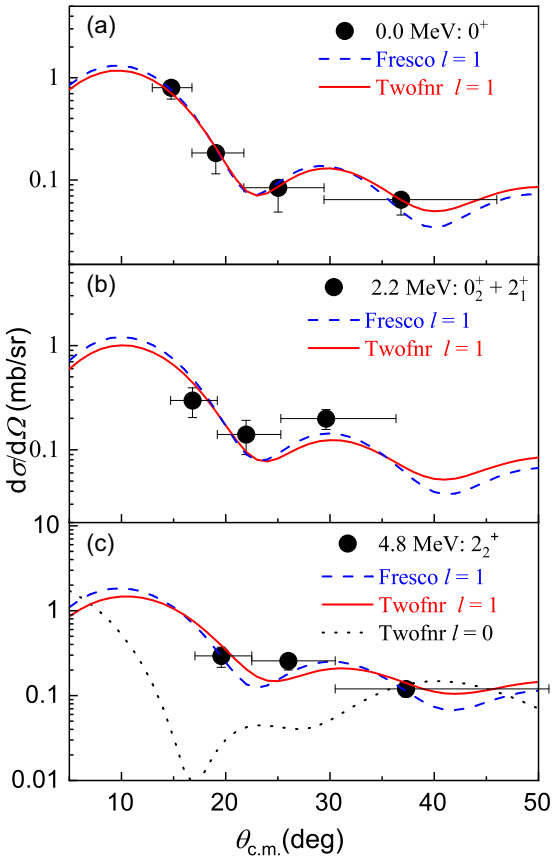

FIG. 10. Differential cross sections of the ^{2}H(^{13}B, ^{3}He)^{12}Be transfer reaction to (a) the 0_1^+, (b) the mixed state of 0_2^+ and 2_1^+, and (c) the 4.8-MeV state in ^{12}Be. The 0_2^+ state can not be separated from the 2_1^+ state, so they were fitted as one peak in Fig. 9. The excitation energies as well as the spin parities of each state in ^{12}Be, and the transferred orbital angular momentum l, which were used in the calculations with the codes of FRESCO and TWOFNR, are given in the figures. Note that the calculation results using the finite-range transfer interactions have been averaged over an angular range corresponding to the angular acceptance for each data point.

consistent with the differential cross sections of this resonance, which is similar to the experimental result of the $1p$ removal reaction [20].

IV. THEORETICAL CALCULATIONS

A. Shell model

Together with the experimental results, the calculated excitation energies and SFs for the related states using various theoretical models are summarized in Table II. The shell model calculations with the YSOX interaction [41] were performed in a full *p-sd* model space. The predictions from Fortune using a simple shell model [27] and Macchiavelli *et al.* with a rotational model [28] are also listed in Table II.

The sum of SFs for $1p$ transitions to all the excited states below 5 MeV is equal to ≈2.5 according to our shell model calculations as well as Fortune's predictions. Therefore, in order to directly compare with the theoretical calculations, the SF_{exp} was normalized to 2.5 and listed in Table II. Note that the second peak in Fig. 9 should have two components that can not be resolved due to the limited experimental resolution. Since the DWBA calculations give almost the same cross sections for the 0_2^+ and 2_1^+ states, the SF in Table II for this peak should correspond to the summation of the SFs for these two excited states. All the calculations predicted a relatively larger SF for the ^{2}H(^{13}B, ^{3}He) reaction to the 2_1^+ state than to the 0_2^+ state. In addition, the SF of the 2_2^+ state is dramatically larger than that of the 0_3^+ state. The excitation energy and the very large SF for the resonant state observed in this experiment are in good agreement with shell model predictions for the second 2^+ state. Therefore, the spin parity of 2^+ was tentatively assigned to this resonance.

B. Gamov coupled channel

The Gamow coupled-channel (GCC) approach was also used to calculate the excitation energy, spin parity, intrinsic width, and configurations of the low-lying states in ^{12}Be. We assumed ^{12}Be as a deformed ^{10}Be core plus two neutrons, and

took into consideration the coupling to the continuum. The interaction and model space in Refs. [16,42] were adopted. The SFs were not calculated for the ^{2}H(^{13}B, ^{3}He) reaction because $^{13}B_{g.s.}$ were not well described by GCC [31]. As listed in Table II, the excitation energy of the newly observed resonance at 4.8 MeV are in line with that of the 2_2^+ and 0_4^+ states predicted at 4.80 and 4.84 MeV, respectively. Both of them are candidates for this new resonance. For the 2_2^+ state, the GCC predicts that two valence neutrons populate p orbitals with a predominant percent $44\%(p_{1/2}p_{1/2}) + 39\%(p_{1/2}p_{3/2})$ but populate the intruder sd orbitals with a very little probability. It is similar to the wave function of ^{12}Be used in shell model to predict the SF of ^{2}H(^{13}B, ^{3}He) [27], so are the 0^+ states. A large SF (1.46) for the 2_2^+ state but a very small SF for the 0^+ state are predicted by various shell model calculations (see Table II). Considering larger experimental SF_{exp} for this new resonance, the 2_2^+ is most probably.

C. Width of the resonance

For the 2_2^+ state, the resonant width of 91 keV predicted by GCC is in good agreement with that of ≈80 keV calculated by Fortune using shell model [24]. However, they are both significantly smaller than the experimental ones observed from the present experiment (0.42 ± 0.28 MeV) and the $1p$ removal reaction (634 ± 60 keV) [20]. Three possible explanations for the experimental width of the $E_n = 1.24$ MeV state were suggested by Fortune: (i) mixed with other states; (ii) decay to the g.s. and the first excited state in ^{11}Be at the same time; (iii) a possible enhancement factor of 1.6 in neutron decays extracted from decay-in-flight experiments [25]. First of all, the 0_3^+ state at 5.565 MeV calculated from our shell model calculations with YSOX interaction is evidently higher than the experimental one. The 0_3^+ (0_4^+) state at $E_x = 4.8$ MeV (4.84 MeV) predicted by Fortune's shell model (GCC), which has not been observed experimentally till now, has a very large probability. Second, as listed in Table II, both shell model and GCC calculations suggest that the excitation energy of the 2^- state is close to the 4.8-MeV resonance. The intrinsic width of 0.814 MeV predicted by GCC has the same order of magnitude as the experimental value of 0–0.43 MeV, demonstrating that it probably corresponds to the 4.44-MeV state observed in the ^{2}H(^{11}Be$_{g.s.}$, p) ^{12}Be reaction [16]. However, it is hard to populate either the $0_3^+/0_4^+$ or the 2^- states in the $1p$ removal/transfer reaction because all their SFs are small (see Table II). Therefore, even if they were populated, the probability would be very small. If the newly observed 4.8-MeV resonance was mixed with a small percent of them, the width would be widened from 80–91 keV to several hundreds keV but the peak position would not change largely. More investigations of $1p$ removal/transfer reaction with better detection resolution in the future are required to clarify whether it is a single or a mixed resonance. The third possibility is able to be easily ruled out because our experiment is not a decay-in-flight experiment.

V. SUMMARY

The low-lying positive-parity states in ^{12}Be were investigated using the ^{2}H(^{13}B, ^{3}He) reaction for the first time with a radioactive beam ^{13}B at 23 MeV/nucleon. Three peaks were obviously populated with the transferred proton angular momentum $l = 1$. The SFs for these three peaks were extracted, which are in reasonable agreement with the shell model predictions. A resonant state at $E_x = 4.8 \pm 0.1$ MeV with a width of 0.42 ± 0.28 MeV was observed. It most likely corresponds to the resonant state with a relative energy of 1.24 ± 0.021 MeV observed from the $1p$ removal reaction, according to its excitation energy, the transferred orbital angular momentum of $l = 1$, as well as its decay path predominated by $1n$. The excitation energy and the SF of this resonance are consistent with predictions from shell model and Gamov coupled channel. The spin parity of 2^+ was tentatively assigned to this resonance. However, its wider decay width requires more investigations with better resolution in the future.

ACKNOWLEDGMENTS

We gratefully thank the RCNP accelerator group for providing ^{18}O primary beam and the RCNP technical staffs for assistance. We also thank Prof. Fortune for helpful discussions about width of the 4.80-MeV state. This work was supported by the National Key R&D Program of China (Grant No. 2018YFA0404403), the National Natural Science Foundation of China (Contracts No. 11775004, No. U1867214, No. 11775013, No. 11775316, No. 11875074, No. 11961141003, and No. U2067205), and the funding from the State Key Laboratory of Nuclear Physics and Technology, Peking University (No. NPT2021ZZ01).

[1] Y. Jin, C. Y. Niu, K. W. Brown, Z. H. Li, H. Hua, A. K. Anthony, J. Barney, R. J. Charity, J. Crosby, D. DellAquila, J. M. Elson, J. Estee, M. Ghazali, G. Jhang, J. G. Li, W. G. Lynch, N. Michel, L. G. Sobotka, S. Sweany, F. C. E. Teh, A. Thomas, C. Y. Tsang, M. B. Tsang, S. M. Wang, H. Y. Wu, C. X. Yuan, and K. Zhu, Phys. Rev. Lett. **127**, 262502 (2021).

[2] A. Ozawa, T. Kobayashi, T. Suzuki, K. Yoshida, and I. Tanihata, Phys. Rev. Lett. **84**, 5493 (2000).

[3] M. Rosenbusch, P. Ascher, D. Atanasov, C. Barbieri, D. Beck, K. Blaum, C. Borgmann, M. Breitenfeldt, R. B. Cakirli, A. Cipollone, S. George, F. Herfurth, M. Kowalska, S. Kreim, D. Lunney, V. Manea, P. Navratil, D. Neidherr, L. Schweikhard, V. Soma, J. Stanja, F. Wienholtz, R. N. Wolf, and K. Zuber, Phys. Rev. Lett. **114**, 202501 (2015).

[4] D. Steppenbeck, S. Takeuchi, N. Aoi, P. Doornenbal, M. Matsushita, H. Wang *et al.*, Nature (London) **502**, 207 (2013).

[5] I. Talmi and I. Unna, Phys. Rev. Lett. **4**, 469 (1960).

[6] B. Zwieglinski, W. Benenson, R. G. H. Robertson, and W. R. Coker, Nucl. Phys. A **315**, 124 (1979).

[7] T. Aumann, A. Navin, D. P. Balamuth, D. Bazin, B. Blank, B. A. Brown, J. E. Bush, J. A. Caggiano, B. Davids, T. Glasmacher, V. Guimaraes, P. G. Hansen, R. W. Ibbotson, D. Karnes, J. J. Kolata, V. Maddalena, B. Pritychenko, H. Scheit, B. M. Sherrill, and J. A. Tostevin, Phys. Rev. Lett. **84**, 35 (2000).

[8] K. T. Schmitt, K. L. Jones, A. Bey, S. H. Ahn, D. W. Bardayan, J. C. Blackmon, S. M. Brown, K. Y. Chae, K. A. Chipps, J. A. Cizewski, K. I. Hahn, J. J. Kolata, R. L. Kozub, J. F. Liang, C. Matei, M. Matos, D. Matyas, B. Moazen, C. Nesaraja, F. M. Nunes, P. D. O'Malley, S. D. Pain, W. A. Peters, S. T. Pittman, A. Roberts, D. Shapira, J. F. Shriner, M. S. Smith, I. Spassova, D. W. Stracener, A. N. Villano, and G. L. Wilson, Phys. Rev. Lett. **108**, 192701 (2012).

[9] Y. Jiang, J. L. Lou, Y. L. Ye, D. Y. Pang, J. Chen, Z. H. Li *et al.*, Chin. Phys. Lett. **35**, 082501 (2018).

[10] H. T. Fortune, G.-B. Liu, and D. E. Alburger, Phys. Rev. C **50**, 1355 (1994).

[11] H. Iwasaki, A. Dewald, C. Fransen, A. Gelberg, M. Hackstein, J. Jolie, P. Petkov, T. Pissulla, W. Rother, and K. O. Zell, Phys. Rev. Lett. **102**, 202502 (2009).

[12] R. Kanungo, A. T. Gallant, M. Uchida, C. Andreoiu, R. A. E. Austin, D. Bandyopadhyay *et al.*, Phys. Lett. B **682**, 391 (2010).

[13] J. G. Johansen, V. Bildstein, M. J. G. Borge, M. Cubero, J. Diriken, J. Elseviers *et al.*, Phys. Rev. C **88**, 044619 (2013).

[14] J. Chen, J. L. Lou, Y. L. Ye, Z. H. Li, D. Y. Pang, C. X. Yuan *et al.*, Phys. Lett. B **781**, 412 (2018).

[15] J. Chen, J. L. Lou, Y. L. Ye, Z. H. Li, D. Y. Pang, C. X. Yuan, Y. C. Ge, Q. T. Li, H. Hua, D. X. Jiang, X. F. Yang, F. R. Xu, J. C. Pei, J. Li, W. Jiang, Y. L. Sun, H. L. Zang, Y. Zhang, G. Li, N. Aoi, E. Ideguchi, H. J. Ong, J. Lee, J. Wu, H. N. Liu, C. Wen, Y. Ayyad, K. Hatanaka, D. T. Tran, T. Yamamoto, M. Tanaka, and T. Suzuki, Phys. Rev. C **98**, 014616 (2018).

[16] J. Chen, S. M. Wang, H. T. Fortune, J. L. Lou, Y. L. Ye, Z. H. Li, N. Michel, J. G. Li, C. X. Yuan, Y. C. Ge, Q. T. Li, H. Hua, D. X. Jiang, X. F. Yang, D. Y. Pang, F. R. Xu, W. Zuo, J. C. Pei, J. Li, W. Jiang, Y. L. Sun, H. L. Zang, N. Aoi, H. J. Ong, E. Ideguchi, Y. Ayyad, K. Hatanaka, D. T. Tran, D. Bazin, J. Lee, Y. N. Zhang, J. Wu, H. N. Liu, C. Wen, T. Yamamoto, M. Tanaka, and T. Suzuki, Phys. Rev. C **103**, L031302 (2021).

[17] R. Meharchand, R. G. T. Zegers, B. A. Brown, S. M. Austin, T. Baugher, D. Bazin, J. Deaven, A. Gade, G. F. Grinyer, C. J. Guess, M. E. Howard, H. Iwasaki, S. McDaniel, K. Meierbachtol, G. Perdikakis, J. Pereira, A. M. Prinke, A. Ratkiewicz, A. Signoracci, S. Stroberg, L. Valdez, P. Voss, K. A. Walsh, D. Weisshaar, and R. Winkler, Phys. Rev. Lett. **108**, 122501 (2012).

[18] S. D. Pain, W. N. Catford, N. A. Orr, J. C. Angelique, N. I. Ashwood, V. Bouchat, N. M. Clarke, N. Curtis, M. Freer, B. R. Fulton, F. Hanappe, M. Labiche, J. L. Lecouey, R. C. Lemmon, D. Mahboub, A. Ninane, G. Normand, N. Soic, L. Stuttge, C. N. Timis, J. A. Tostevin, J. S. Winfield, and V. Ziman, Phys. Rev. Lett. **96**, 032502 (2006).

[19] A. Navin, D. W. Anthony, T. Aumann, T. Baumann, D. Bazin, Y. Blumenfeld, B. A. Brown, T. Glasmacher, P. G. Hansen, R. W. Ibbotson, P. A. Lofy, V. Maddalena, K. Miller, T. Nakamura, B. V. Pritychenko, B. M. Sherrill, E. Spears, M. Steiner, J. A. Tostevin, J. Yurkon, and A. Wagner, Phys. Rev. Lett. **85**, 266 (2000).

[20] J. K. Smith, T. Baumann, D. Bazin, J. Brown, S. Casarotto, P. A. DeYoung, N. Frank, J. Hinnefeld, M. Hoffman, M. D. Jones, Z. Kohley, B. Luther, B. Marks, N. Smith, J. Snyder, A. Spyrou, S. L. Stephenson, M. Thoennessen, N. Viscariello, and S. J. Williams, Phys. Rev. C **90**, 024309 (2014).

[21] D. E. Alburger, S. Mordechai, H. T. Fortune, and R. Middleton, Phys. Rev. C **18**, 2727 (1978).

[22] H. G. Bohlen, W. von Oertzen, T. Kokalova, C. Schulz, R. Kalpakchieva, T. N. Massey, and M. Milin, Int. J. Mod. Phys. E **17**, 2067 (2008).

[23] H. T. Fortune, Phys. Rev. C **88**, 039801 (2013).

[24] H. T. Fortune, Phys. Rev. C **93**, 034325 (2016).

[25] H. T. Fortune, Eur. Phys. J. A **52**, 11 (2016).

[26] H. T. Fortune, Phys. Rev. C **98**, 024322 (2018).

[27] H. T. Fortune, Phys. Lett. B **755**, 351 (2016).

[28] A. O. Macchiavelli, H. L. Crawford, C. M. Campbell, R. M. Clark, M. Cromaz, P. Fallon, M. D. Jones, I. Y. Lee, and M. Salathe, Phys. Rev. C **97**, 011302 (2018).

[29] T. Shimoda, H. Miyatake, and S. Morinobu, Nucl. Instrum. Methods Phys. Res., Sect. B **70**, 320 (1992).

[30] H. J. Ong, AIP Conf. Proc. **1588**, 146 (2014).

[31] W. Liu, J. L. Lou, Y. L. Ye, Z. H. Li, Q. T. Li, H. Hua, X. F. Yang, J. Y. Xu, H. J. Ong, D. T. Tran, N. Aoi, E. Ideguchi, D. Y. Pang, C. X. Yuan, S. M. Wang, Y. Jiang, B. Yang, Y. Liu, J. G. Li, Z. Q. Chen, J. X. Han, S. W. Bai, G. Li, K. Ma, Z. W. Tan, H. Y. Zhu, and B. L. Xia, Phys. Rev. C **104**, 064605 (2021).

[32] S. Agostinelli, J. Allison, K. Amako, J. Apostolakis, H. Araujo, P. Arce *et al.*, Nucl. Instrum. Methods Phys. Res. A **506**, 250 (2003).

[33] J. Chen, J. L. Lou, Y. L. Ye, J. Rangel, A. M. Moro, D. Y. Pang, Z. H. Li, Y. C. Ge, Q. T. Li, J. Li, W. Jiang, Y. L. Sun, H. L. Zang, Y. Zhang, N. Aoi, E. Ideguchi, H. J. Ong, J. Lee, J. Wu, H. N. Liu, C. Wen, Y. Ayyad, K. Hatanaka, T. D. Tran, T. Yamamoto, M. Tanaka, T. Suzuki, and T. T. Nguyen, Phys. Rev. C **94**, 064620 (2016).

[34] RIBLL Collaboration, Y. Jiang, J. L. Lou, Y. L. Ye, Y. Liu, Z. W. Tan, W. Liu, B. Yang, L. C. Tao, K. Ma, Z. H. Li, Q. T. Li, X. F. Yang, J. Y. Xu, H. Z. Yu, J. X. Han, S. W. Bai, S. W. Huang, G. Li, H. Y. Wu, H. L. Zang, J. Feng, Z. Q. Chen, Y. D. Chen, Q. Yuan, J. G. Li, B. S. Hu, F. R. Xu, J. S. Wang, Y. Y. Yang, P. Ma, Q. Hu, Z. Bai, Z. H. Gao, F. F. Duan, L. Y. Hu, J. H. Tan, S. Q. Sun, Y. S. Song, H. J. Ong, D. T. Tran, D. Y. Pang, and C. X. Yuan, Phys. Rev. C **101**, 024601 (2020).

[35] W. W. Daehnick, J. D. Childs, and Z. Vrcelj, Phys. Rev. C **21**, 2253 (1980).

[36] Y. Zhang, D. Y. Pang, and J. L. Lou, Phys. Rev. C **94**, 014619 (2016).

[37] I. J. Thompson, Comput. Phys. Rep. **7**, 167 (1988).

[38] J. Tanaka, R. Kanungo, M. Alcorta, N. Aoi, H. Bidaman, C. Burbadge *et al.*, Phys. Lett. B **774**, 268 (2017).

[39] http://nucleartheory.eps.surrey.ac.uk/NPG/index.htm

[40] D. Y. Pang, P. Roussel-Chomaz, H. Savajols, R. L. Varner, and R. Wolski, Phys. Rev. C **79**, 024615 (2009).

[41] C. X. Yuan, T. Suzuki, T. Otsuka, F. R. Xu, and N. Tsunoda, Phys. Rev. C **85**, 064324 (2012), 1209.5587.

[42] S. M. Wang, W. Nazarewicz, R. J. Charity, and L. G. Sobotka, Phys. Rev. C **99**, 054302 (2019).